Multisided Linear Induction Generator, Analytical Modeling, 3-D Finite Element Analysis and Experimental Test

M. Hosseini Aliabadi[1], S. H. Hosseinian[2], S. J. Moghani[2], M. Abedi[2]
[1] *Department of Electrical Engineering, Science and Research Branch, Islamic Azad University, Tehran, Iran*
[2] *Department of Electrical Engineering, Amirkabir University of Technology, Tehran, Iran*
m.h.aliabadi@srbiau.ac.ir

***Abstract*—In this paper, a new generator for converting of sea wave energy to electrical energy is proposed. At the beginning, analytical model of generator is extracted and then 3-D and 2-D finite element analysis (FEA) have been developed and implemented on the dodecahedron tubular linear induction motor/generator. The generator have been studied in normal and heavy weather condition in Persian Gulf and sensitivity analysis of the generator against sea wave period and height on the voltage, efficiency and thrust is studied. The results verify the accuracy of self–excited tubular linear induction generator (SETLIG) model and show that tubular linear induction generator can be used as a powerful tool for converting of wave energy to electrical energy.**

***Index Terms*—Linear induction motor, linear induction generator, wave energy, sensitivity analysis.**

I. INTRODUCTION

A serious effort to make an effective technology began from midst of the 1970 and the proposed programs for extraction of energy from sea and ocean waves are sponsored by many countries. Different types of generators are mostly used in wave energy extraction system. Permanent magnet synchronous generators (PMSG) are investigated in [1]–[10]. Demagnetization of permanent magnet and not to be any control on field is the main drawbacks of PMSG. Air core generators have been developed in [11]. In spite of simple structure and low construction cost of this generator, its efficiency is very low and thereby it is not suitable choice for wave energy conversion.

Due to aforementioned drawbacks regarding permanent magnet and air core generators, induction generators shall be taken into consideration for conversion of wave and tidal energy into electrical energy. The noticeable advantages of induction generator are: 1) low maintenance cost; 2) rigid structure; 3) easy construction; 4) wide range application.

Among the induction generators, linear induction generators are preferred to the rotary type due to elimination of mechanical equipment interface such as gear box and lube by unrolling a rotating induction generator with a radial emi-plane and winding to obtain tubular linear induction generator illustrated in Fig. 1.

The main advantage of the TLIGs is: they are rugged and easy to construct [12]. The former is assembled in (four, six to twelve) separate cores and may be considered as several flat LIGs. So, it is more difficult to build than a flat linear induction generator. The thrust on the moving part of a TLIG is generated by the electromagnetic interaction between the radial oriented translating magnetic field and the circular induced current on the moving part.

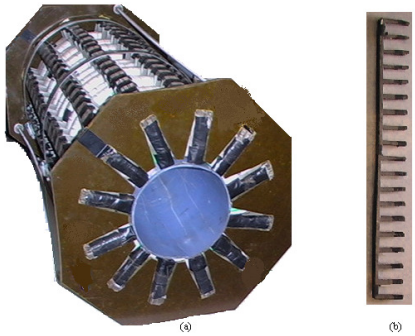

Fig. 1. Longitudinally-laminated TLIG: (a) front view of generator, (b) stator lamination.

Many researches magnetically analyzed the operation of linear induction machine [13]–[16], but in standstill application, it is not developed very well. In this paper the analytical and numerical approximation of a force imposed on conducting section of motor/generator is developed. A theoretical approach of the system is presented. Finite element model and related simulations of system are described. Experimental tests are arranged and comparisons among empirical data, analytical model and finite element methods have been presented.

II. SYSTEM MODELLING

A. System's configuration

Figure 2 shows how the sea energy can be achieved using linear generators. This configuration consists of a buoy coupled by a rope, directly to the piston. The piston is

Manuscript received August 7, 2012; accepted Febraury 1, 2013.
This research was supported by Islamic Azad university, science and research branch.

connected via spring to concrete foundation that is fixed in the bottom of the sea. The tension of the rope will be balanced with the above mentioned spring. The piston will move up and down approximately with the wave and tidal speed.

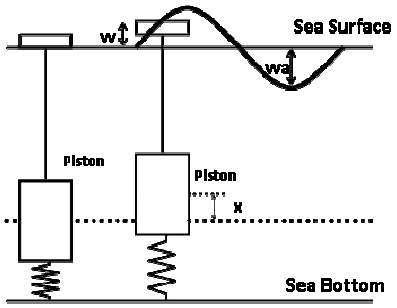

Fig. 2. General outline of direct drive energy extraction system.

A cross sectional view of a TLIG used as sea wave energy convertor is shown in Fig. 3.

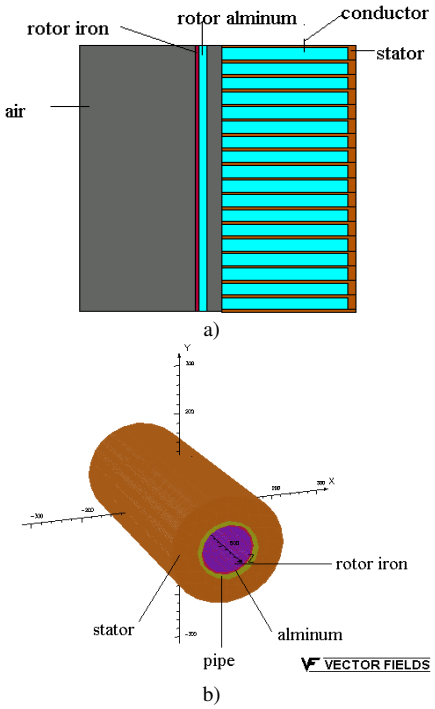

Fig. 3. Tubular linear induction generator: (a) cross section, (b) three-dimensional model.

III. STANDSTILL OPERATION ANALYSIS

The induction machine imposes a sliding linear current density defined by (1) [12]

$$\mathbf{J}_e = \mathbf{J}_m e^{j(wt-kx)}, \tag{1}$$

where $\mathbf{J}$, w and k are current density, angular frequency and machine wave constant respectively. The system parameters have been driven from the laboratorial prototype. The related parameters of the TLIG are listed in Table I.

B. Bi dimensional analysis

Considering the Fig. 3(a), the z component of the flux density is zero ($\mathbf{b}_z = 0$) and the current density has only the z component ($\mathbf{j}_x = \mathbf{j}_y = 0$).

TABLE I.TUBULAR LINEAR INDUCTION GENERATOR PARAMETERS

Parameter	Quantity
Number of phases	3
Number of coil/phase/pole	1
Number of turns/coil	90
Pole pitch	84 mm
Coil-pitch	84 mm
Current supply	14.6 A (r.m.s)
Rotor aluminum thickness	3 mm
Rotor iron thickness	1.6 mm
Coil thickness	23 mm
Teeth thickness	5 mm
Inner stator diameter	114 mm
Number of poles	6
Length of generator	510 mm

Using this fact that flux density is zero in z direction and current density is zero in x and y directions, the force density will have x and y components and is zero in z direction. Force density distribution in the conductor is obtained by (2)–(4):

$$\mathbf{f} = \mathbf{j}\times\mathbf{b}, \tag{2}$$

$$\mathbf{f} = \mathbf{j}\times\mathbf{b} = \underbrace{(j_y b_z - j_z b_y)}_{F_x}\mathbf{u}_x + \underbrace{(j_z b_x - j_x b_z)}_{F_y}\mathbf{u}_y + \underbrace{(j_x b_y - j_y b_x)}_{F_z}\mathbf{u}_z, \tag{3}$$

$$\mathbf{f} = -(j_z b_y)\mathbf{u}_x + (j_z b_x)\mathbf{u}_y = F_x\mathbf{u}_x + F_y\mathbf{u}_y, \tag{4}$$

where $\mathbf{b}$ is magnetic flux density and x,y,z are Cartesian Axis's direction. The magnetic vector potential A can be employed to obtain the electromagnetic equations needed for a complete description of the system. The distribution of the magnetic vector potential is given by (5)

$$\frac{\partial^2 \mathbf{A}_z}{\partial x^2} + \frac{\partial^2 \mathbf{A}_z}{\partial y^2} - \mu\sigma v_x \frac{\partial \mathbf{A}_z}{\partial x} - \mu\sigma \frac{\partial \mathbf{A}_z}{\partial t} = 0. \tag{5}$$

The solution of (5) is given by (6)

$$\mathbf{A}_z(x, y, t) = \mathbf{A}(y) e^{j(wt-kx)}. \tag{6}$$

Substituting (5) in (6) results following differential equation

$$\frac{d^2 \mathbf{A}}{dy^2} - [k^2 + j\mu\sigma w]\mathbf{A} = 0. \tag{7}$$

Therefore $A(y)$ is

$$\mathbf{A}(y) = C_1 e^{\beta y} + C_2 e^{-\beta y}, \tag{8}$$

where $\beta = \sqrt{k^2 + j\mu\sigma w}$, μ, σ are permeability and conductivity constants, $C1$, $C2$, β are equation constants respectively. Eventually **A** is obtained from (9)

$$\mathbf{A} = (C_1 e^{\beta y} + C_2 e^{-\beta y}) e^{j(wt-kx)} \mathbf{u}_z. \quad (9)$$

Using two boundary conditions, equation (9) can be solved. First condition is obtained by neglecting the air gap between stator and conductor for simplicity Fig. 4.

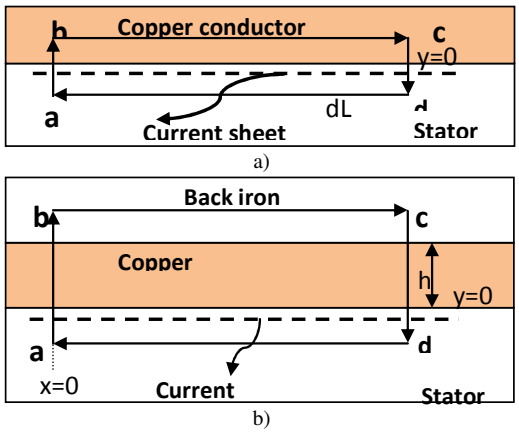

Fig. 4. First boundary condition at y=0 (a); second boundary condition including the current density in the conductor from y = 0 to y = h (b).

From (9) and with considering the fact that the contour can be chosen small enough, the magnetic field does not vary appreciably over its length. Based on Fig. 4(a) at y=0, magnetic field intensity is obtained by (10)

$$\int_a^b \mathbf{H}_x dx + \int_b^c \mathbf{H}_y dy + \int_c^d \mathbf{H}_x dx + \int_d^a \mathbf{H}_y dy = \int_a^b \mathbf{j}_e dx, \quad (10)$$

$$\mathbf{H}_x = -\mathbf{j}_e, \quad (11)$$

$$\mathbf{b}_x = \frac{\partial \mathbf{A}_z}{\partial y} = -\mu \mathbf{j}_e \; at \; y = 0. \quad (12)$$

Substituting (9) in latter equation from (6), the subsequent formula is derived

$$C_2 - C_1 = \frac{\mu \mathbf{j}_m}{\beta}. \quad (13)$$

Applying second boundary condition, Fig. 4(b), leads to (14)

$$\int_a^b \mathbf{H}_y dy + \int_c^d \mathbf{H}_y dy = -\int_a^d \mathbf{j}_E dx - \int_0^h \int_a^d \mathbf{j}_z dx dy. \quad (14)$$

From $\mathbf{H}_y = -\frac{1}{\mu}\frac{\partial \mathbf{A}_z}{\partial x}$

$$\mathbf{H}_y = \frac{jk}{\mu}(C_1 e^{\beta y} + C_2 e^{-\beta y}) e^{j(wt-kx)}. \quad (15)$$

The current density $\mathbf{j}_z$ satisfies $-1/\mu \nabla^2 \mathbf{A} = 0$ which gives

$$\mathbf{j}_z = \frac{(k^2 - \beta^2)}{\mu}(C_1 e^{\beta y} + C_2 e^{-\beta y}) e^{j(wt-kx)}. \quad (16)$$

So second equation of C_1, C_2 is

$$[C_1(e^{\beta h} - 1) - C_2(e^{-\beta h} - 1) = \frac{\mu \mathbf{j}_m}{\beta}. \quad (17)$$

Using (13) and (17), C1 and C2 will be presented by:

$$C_1 = \frac{\mu \mathbf{j}_m e^{-\beta h}}{\beta(e^{\beta h} - e^{-\beta h})}, \quad (18)$$

$$C_2 = \frac{\mu \mathbf{j}_m e^{\beta h}}{\beta(e^{\beta h} - e^{-\beta h})}. \quad (19)$$

This formula can be used to obtain the magnetic vector potential distribution, magnetic field density and current density:

$$\mathbf{A} = \frac{\mu \mathbf{j}_m (e^{\beta(y-h)} + e^{\beta(h-y)})}{\beta(e^{\beta h} - e^{-\beta h})} e^{j(wt-kx)} \mathbf{u}_z, \quad (20)$$

$$\mathbf{H} = \frac{\mathbf{j}_m (e^{\beta(y-h)} - e^{\beta(h-y)})}{\beta(e^{\beta h} - e^{-\beta h})} e^{j(wt-kx)} \mathbf{u}_x + j\frac{\mathbf{j}_m (e^{\beta(y-h)} + e^{\beta(h-y)})}{\beta(e^{\beta h} - e^{-\beta h})} e^{j(wt-kx)} \mathbf{u}_y, \quad (21)$$

$$\mathbf{j} = \frac{j_m (k^2 - \beta^2)(e^{\beta(y-h)} + e^{\beta(h-y)})}{\beta(e^{\beta h} - e^{-\beta h})} e^{j(wt-kx)} \mathbf{u}_z. \quad (22)$$

Based on (4), force can be calculated as follows

$$\mathbf{f} = -k\mu \mathbf{j}_m^2 \mathrm{Re}[\frac{(k^2 - \beta^2)(e^{\beta(y-h)} + e^{\beta(h-y)})}{\beta(e^{\beta h} - e^{-\beta h})} \times e^{j(wt-kx)}] \times \mathrm{Re}[j\frac{(e^{\beta(y-h)} + e^{\beta(h-y)})}{\beta(e^{\beta h} - e^{-\beta h})} \times e^{j(wt-kx)}] \mathbf{u}_x + \mu \mathbf{j}_m^2 \mathrm{Re}[\frac{(k^2 - \beta^2)(e^{\beta(y-h)} + e^{\beta(h-y)})}{\beta(e^{\beta h} - e^{-\beta h})} \times e^{j(wt-kx)}] \times \mathrm{Re}[j\frac{(e^{\beta(y-h)} - e^{\beta(h-y)})}{e^{\beta h} - e^{-\beta h}} e^{j(wt-kx)}] \mathbf{u}_y. \quad (23)$$

Because of TLIG's structure, cylindrical coordination is preferred to obtain magnetic vector potential as

$$\frac{\partial^2 \mathbf{A}_\theta}{\partial z^2} + \frac{\partial^2 \mathbf{A}_\theta}{\partial r^2} + \frac{1}{r}\frac{\partial \mathbf{A}_\theta}{\partial r} - \frac{\mathbf{A}_\theta}{r^2} = -\mu \mathbf{j}_\theta. \quad (24)$$

Within the stator slots $j_\theta = j_s$ and within the air gap and the iron regions: $\mathbf{j}_\theta = 0$. Within the rotor aluminum or copper region (conductor region): $\mathbf{j}_\theta = \mathbf{j}_r$. In Tubular linear induction machine, the flux density along the θ axis and the current densities along the z and r axes are approximately equal to zero as shown in Fig. 7, Fig. 8. Therefore, in this

machine the non-zero force is only available in the z direction. The z-direction force F_z can be calculated from the following equation

$$\mathbf{f}_z = \int_v (\mathbf{j}\times\mathbf{b})dv = 2\pi\int r(\mathbf{j}\times\mathbf{b})ds. \quad (25)$$

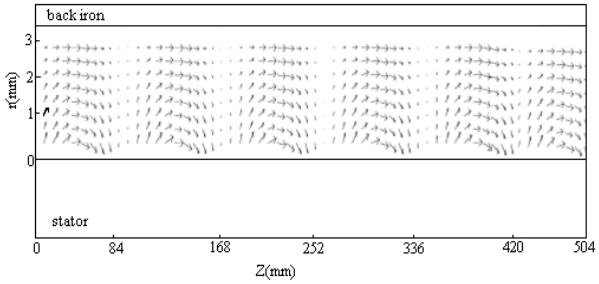

Fig. 5. Distribution of Force in conductor.

Based on analytical model, distribution of force density in the conductor has been shown in Fig. 5. It shows that the force is distributed along the Z direction and makes rotor to move from standstill.

IV. Two and Three Dimensional Finite Element Simulations

The mentioned machine is analyzed with 2-D FEM and the resultant flux density distribution is shown in Fig. 6. The number of elements is 59661, which is about half of the amount used in a 3-D analysis.

TABLE II. COMPARISON BETWEEN 2-D AND 3-D FINITE ELEMENT ANALYSIS

	2-D FEM	**3-D FEM**
Force obtained (N)	158	180
Number of elements	59661	117975
Needed time (s)	1343	2927

The comparison between 2-D and 3-D finite element analysis has been shown in Table II.

The force resulted from the 2-D FEM simulation is 158 Newton, which does not compare well with the measured value of 175 Newton. Flux density at 2-D FEM analysis has been shown in Fig.6, which R and Z are the axis in the cylindrical coordinate. The force resulting from the 3-D analysis is 180 Newton, which compares very well with the experimental value. The analysis time in 2-D and 3-D simulation, using a Pentium IV is 1343 and 2927 seconds respectively.

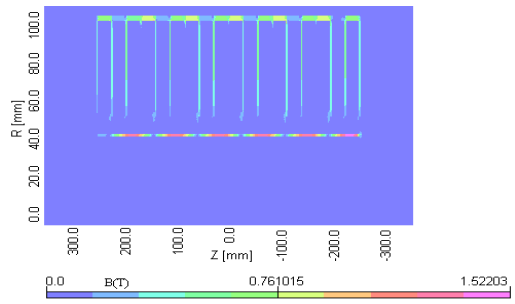

Fig. 6. Flux density at 2-d Fem analysis.

As stated above because of structure of the TLIG, flux and current density only exists in θ direction and in z and r direction is null. This is demonstrated by 3-D FEM and is showed in Fig. 7 and Fig. 8 respectively.

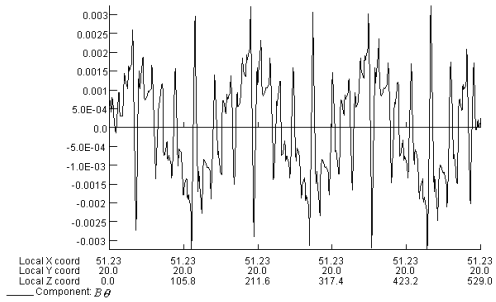

Fig. 7. Flux density along θ direction.

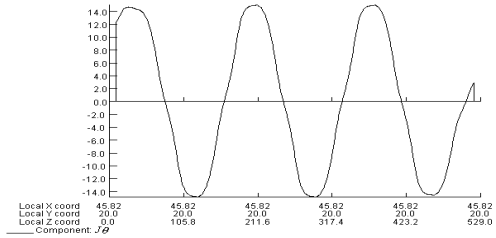

Fig. 8. The current density (A/mm^2) versus θ.

Figure 9 shows the standstill thrust variations. The electrical angle step width at each time step is 10 degree. This result has been derived from 3-D finite element Analysis.

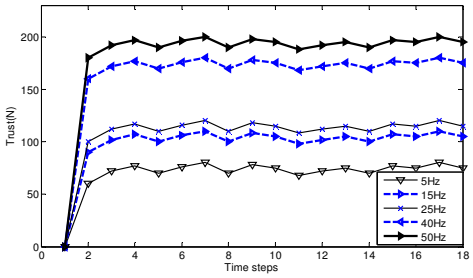

Fig. 9. 3-D Standstill thrust in time steps.

Figure 10 shows the characteristics of standstill thrust of the analyzed model, which are the steady state average values of the thrusts in Fig. 9. The calculated results match very well with the measured ones.

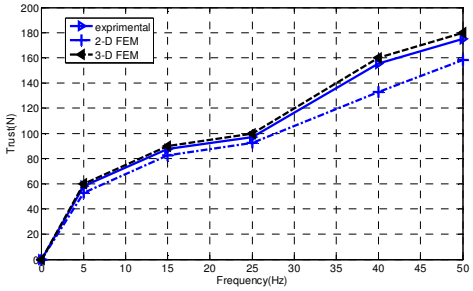

Fig. 10. Standstill thrust characteristics with frequency variation.

V. Simulation of TLIG as Wave Energy Converter

When the generator has been studied in motor mode and magnetically analyzed well, in this section it is used as a

wave energy converter (Fig. 2).In the present study, waves are considered large, the wave height is 3 meters and the wave period is 4 seconds. These kinds of waves take place at the wide area of the Persian Gulf. The direct drive generator and the buoy are sized according to the wave parameters. Spring is sized to have equal energy at the upward and downward piston motion. The piston is chosen 296 mm longer than the stator to achieve effective electricity production. The studies have been done for the generator nominal parameters and then sensitivity analyses have been made under different conditions.

A. Normal condition

Normal condition means that the waves are sinusoidal. All the forces imposed on wave convertor are presented in Fig. 11. As it is shown, end stop force is zero because the condition is considered to be normal.

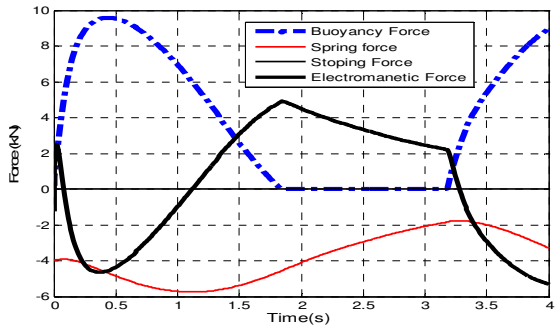

Fig. 11. Force acting in systems in normal condition.

The piston and wave speed of a 7-kVA linear induction generator is shown in Fig. 12. The solid lines refer to the wave and the dashed lines to the piston. The simulations are done over one wave period.

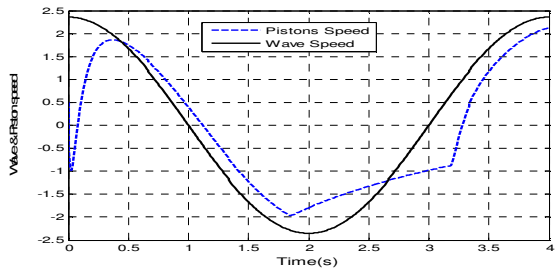

Fig. 12. Wave and piston speed in normal condition.

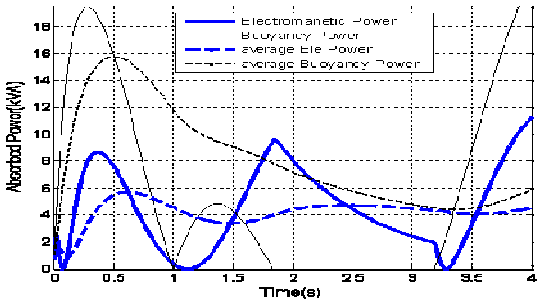

Fig. 13. Buoy and electromagnetic power.

Figure 13 indicates the main important extracted power from the buoy and also electromagnetic forces. The downward and upward electromagnetic power (output power) is nearly equal. This means that the spring is chosen suitable and retracts the piston with necessary speed.

B. Heavy weather condition

Heavy weather condition means the sea is not calm and any sudden changes such as storm and hurricane is expected. In this situation to prevent of generator damage, the stop force will act and behaviors of all forces are as Fig.14.

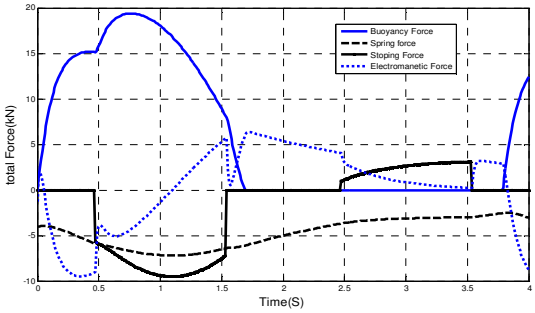

Fig. 14. Force acting in systems in heavy weather condition.

As it can be seen, the stop force is not zero in the system. Also the electromagnetic reaction of the generator is different in comparison with normal condition. The spring forces are higher than the normal condition. In heavy condition the buoyancy force is about two times more than normal condition.

As it is expected, the absorbed power from the wave in this condition is more than the normal condition. Figure 15 confirms this matter. In this condition the absorbed power of the generator sometimes reaches to zero because stop force will act in heavy condition.

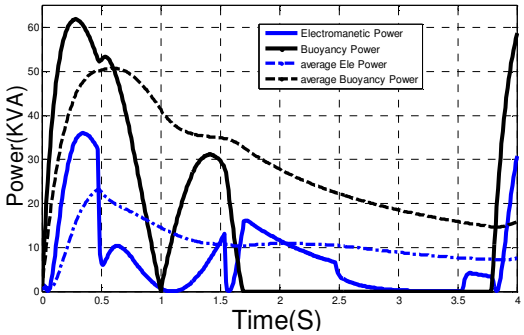

Fig. 15. Buoy and electromagnetic power in heavy condition.

In heavy weather condition as it is shown in Fig. 16, piston has a variable speed and does not follow the wave speed.

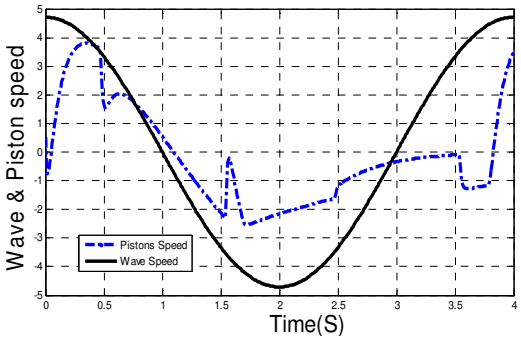

Fig. 16. Wave and piston speed in heavy condition.

VI. SENSITIVITY ANALYSIS OF GENERATOR

Performance of the DTLIG has been affected by many

factors and variables like piston velocity, slip value, wave period and wave height that directly effects on output voltage, efficiency and force.

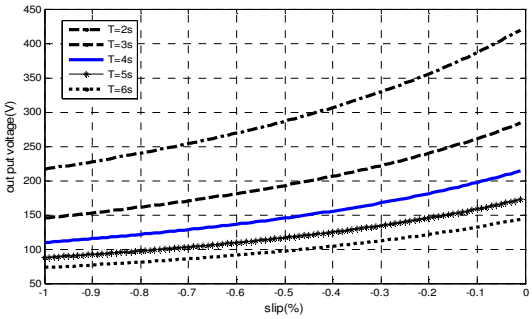

Fig. 17. Wave period variation effect on voltage.

Figure 17 shows the variation of output voltage with wave period. As it can be seen, by increasing the wave period, the output voltage will decrease.

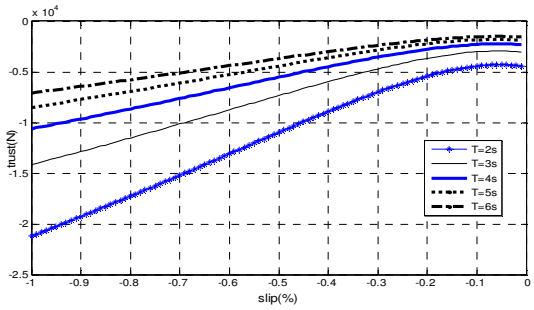

Fig. 18. Wave period variation effect on Trust.

The variation of efficiency by wave height and period versus slip is negligible. Increasing and decreasing of wave period has not many effect on efficiency. Figure 18 shows the variation of thrust force with wave period. As it is shown, by increasing the wave period, the thrust force will decrease. At the desired wave period (T=4 s) and slip (s=10 %), the thrust force will be about 2300 N. As it is expected, near the working points the variation of thrust with wave period is less but whatever we close to unstable region(s = -1), such variant get more.

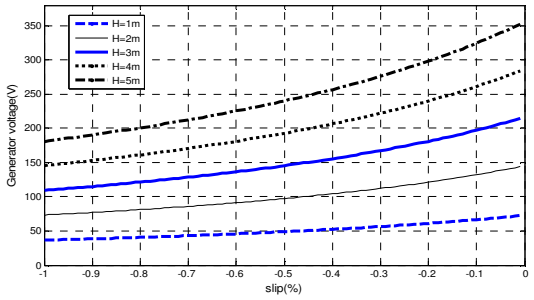

Fig. 19. Wave height variation effect on voltage.

Figure 19 shows the variation of generator voltage with wave height. As it is shown, by increasing the wave period the voltage increases. At the desired wave height (H=3m) and slip (s = 10 %), the generator voltage is 200 V that is comparable with a calculated one.

Figure 20 shows the variation of thrust force with wave height. As it is shown, by increasing the wave height, the thrust force increases. At the desired wave height (H = 3 m) and slip (s = 10 %), the thrust force will be about 2300 N. As it is expected, near the working points the variation of thrust with wave height is low but whatever we close to unstable region(s = -1), such variant get more.

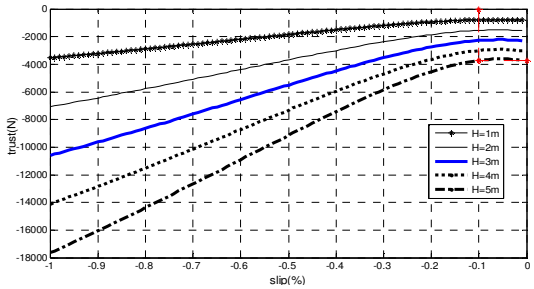

Fig. 20. Wave height variation effect on Trust.

VII. EXPERIMENTAL RESULT OF DTLIG

According to the topology of the magnetic circuit, the stator of mentioned DTLIG has longitudinal lamination. It is assembled in twelve separate cores and makes a dodecahedron TLIG. The motor described in above sections was used in the laboratory to test. The speed of the test machine was varied using a rotating induction motor with the nominal power of 6 kW and nominal voltage of 380 V that are connected to the piston of the generator via prototyped interface equipment shown in Fig. 21.

Fig. 21. Prototyped interface equipment.

The test is done when the rotary induction motor is connected to the linear induction generator via interface equipment (Fig. 22). When the induction generator with capacitance connected at its stator terminals, is driven by a prime mover, such as a sea wave and tidal, voltage will start to develop at a corresponding minimum speed. The minimum speed and capacitance measured for self-excitation and voltage built up are 1.5 m/s and 800 μF respectively.

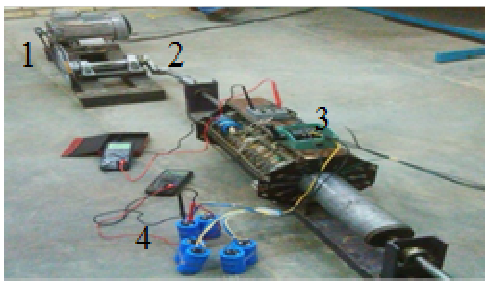

Fig. 22. Experimental set up for energy conversion system 1-rotary induction motor 20 interface equipment 3) linear induction generator 4) terminal capacitance.

TABLE III: PEAK PHASE VOLTAGE COMPARISON

Method	Experimental	FEM	Analytical
Voltage (V)	179.8	188	197
Error (%)	-	4	9

After the self-excitation, the steady state voltage at the generator terminal has been measured and compared with the analytical and finite element method. Table III shows voltages obtained by different method.

VIII. CONCLUSIONS

In this paper, Tubular linear induction motor/generator has been investigated. First, the machine has been analyzed in motoring mode analytically and the performance of the machine verified by finite-element's method. Then machine used as a generator in the wave energy conversion system. In this application, the generator performance studied in normal and heavy weather condition in Persian Gulf and sensitivity analysis of the generator against sea wave period and height on the voltage and thrust is studied. The study shows that increasing and decreasing of wave height and period, seriously effects on voltage and trust. For more verification the generator is tested in laboratory and output voltage obtained and compared with the analytical and finite element results. The results show that tubular linear induction generator can be used as powerful tool in wave energy extraction system.

REFERENCES

[1] M. Nikolaos, Kimoulakis, *et al*, "Cogging Force Minimization in a Coupled Permanent Magnet Linear Generator for Sea Wave Energy Extraction Applications", *IEEE Trans On Magnetics*, vol. 45, no. 3, Mar. 2009.

[2] C. Boström, *et al*, "Peer-Reviewed Technical Communication-Study of a Wave Energy Converter Connected to a Nonlinear Load", *IEEE Journal Of Oceanic Engineering,* vol. 34, no. 2, Apr. 2009. [Online]. Available: http://dx.doi.org/10.1109/JOE.2009.2015021

[3] M. Leijon, *et al*, "Economical consideration of renewable electric energy production–especially development of wave energy", *Renewable Energy,* Elsevier, pp. 1201–09, 2003.

[4] S. Loránd, *et al*, "Novel Permanent Magnet Tubular Linear Generator for Wave Energy Converters", Department of Electrical Machines, Technical University of Cluj, Romania

[5] M. Leijon, *et al*, "An electrical approach to wave energy", *Renewable energy,* Elsevier, pp. 1309–1319, 2006.

[6] A. I. Ivanova, *et al,* "Simulation of Wave-Energy Converter With Octagonal Linear Generator", *IEEE Journal of Oceanic Engineering*, vol. 30, no. 3, pp. 619–629, July 2005. [Online]. Available: http://dx.doi.org/10.1109/JOE.2005.858373

[7] M. Leijon, *et al*, "Multiphysics Simulation of Wave Energy to Electric Energy Conversion by Permanent Magnet Linear Generator", *IEEE Trans. Energy conversion*, vol. 20, no. 1, Mar. 2005

[8] I. A. Ivanova, *et al*, "Simulated generator for wave energy extraction in deep water", *Ocean engineering*, Elsevier, no. 32, 2005.

[9] P. Zheng, *et al*, "Research on a Tubular Longitudinal Flux PM Linear Generator Used for Free-Piston Energy Converter", *IEEE Trans. Magnetics*, vol. 43, no. 1, Jan. 2007.

[10] W. N. L. Mahadi, S. R. Adi, Wijono, "Application of ND2FE14B magnet in the linear generator design", *Int. Journal of Engineering and Technology*, vol. 4, no. 2, pp. 175–184, 2007.

[11] L. Szabó, *et al*, "Wave Energy Plants for the Black Sea – Possible Energy Converter Structures", in *Proc. of ICCEP,* Capri, 2007.

[12] S. A. Nasar, *Linear Motion Electric Machines*, NY: Wiley, 1976.

[13] N. Tavana. *et al*, "Performance Improvement of Linear Permanent-Magnet Synchronous Motor with Halbach Array", *IREE*, vol. 4, no. 6, pp. 1210–1214, 2009.

[14] A. H .Bagegni, *et al*, "Tubular Linear Induction Motor Capsule Pipeline – Part1: Finite Element Analysis", *IEEE Trans. Energy Conversion*, vol. 8, no. 2, pp. 257–262, 1993. [Online]. Available: http://dx.doi.org/10.1109/60.222716

[15] S. Poitout, et al, "Theoretical Modeling and Experimental Tests of an Electromagnetic Fluid Transportation System Driven by a Linear Induction Motor", *IEEE Trans. Magnetics,* vol. 42, no. 9, pp. 2133–2151, 2006. [Online]. Available: http://dx.doi.org/10.1109/TMAG.2006.880396

[16] M. Jafarboland, A. Nekoubin, "Design and Optimization of a Double-Sided Linear Induction Motor Based on Finite Element Method", *Int. Review of Electrical Engineering*, vol. 5, no. 3, pp. 961–969, 2010.